Solid Freeform Fabrication 2024: Proceedings of the 35th Annual International Solid Freeform Fabrication Symposium – An Additive Manufacturing Conference
Reviewed Paper

GEOMETRIC REPEATABILITY STUDY FOR ROBOTIC WAAM OF ALUMINUM

K. M. Sargent*, H. R. Peters*, J. J. Penney*, and T. L. Schmitz*

*Department of Mechanical, Aerospace, and Biomedical Engineering,

University of Tennessee, Knoxville, TN, 37923

Abstract

This paper evaluates the geometric repeatability of components printed by robotic wire arc additive manufacturing (WAAM). The WAAM system includes a KUKA KR 50 R2500 robot and a Fronius CMT Advanced 4000 welder. Gas metal arc welding (GMAW) is used for layer-by-layer deposition of ER4943-aluminum wire. A single geometry is printed five times using the same part plan, weld settings, and wire. The geometric repeatability is then evaluated. Each component is measured using structured light scanning, 3D models are generated, and the deviations between prints are determined. Experimental results are provided, comparisons are performed, and conclusions are drawn.

Introduction

WAAM is a direct energy deposition (DED) additive manufacturing (AM) process that is becoming more broadly implemented in production environments. Due to higher deposition rates than other AM processes, robotic welding capabilities, and availability of large metal wire spools, large metal components can be 3D printed [1]. WAAM utilizes gas metal arc welding to deposit metal in a layer-by-layer process. Robotic WAAM allows for constant travel speeds with increased maneuverability. During deposition, metal wire is motor driven at a constant, optimized feed rate through the welding torch.

Large complex geometries are traditionally produced by casting or forging, but there is currently a lack of US infrastructure for large components and lengthy lead times for offshore production. To address this issue, WAAM can be applied to print large volume parts with low production quantities. Because lightweight materials, such as aluminum, with high strength, high ductility, and good corrosion resistance are desirable in aerospace and marine applications [2], these industries are key candidates for WAAM.

Aluminum WAAM

Aluminum alloys have high thermal conductivity, high strength, good corrosion resistance, and low density. They are also less expensive than advanced metals such as titanium alloys. Because aluminum is weldable, it is well-suited for WAAM. Deposition rates for aluminum can range from 1 kg/hr to 4 kg/hr [3]. Challenges associated with WAAM for aluminum alloys are porosity, temperature defects, layer height inconsistencies, and build plate deformation [4] [5]. Porosity can affect the mechanical properties and mostly occurs due to inadequate shielding gas coverage or improper fusion between layers. Temperature defects can affect the fusion of each layer or cause sagging to occur. With aluminum, appropriate interpass temperature (i.e., the temperature of the base material before the next layer is deposited) is critical to ensure a consistent bead profile and layer height. Too high or too low interpass temperatures can create varying layer heights, which then directly affect the path planned for deposition. To avoid this, the interpass temperature should be monitored to provide sufficient cooling between layers.

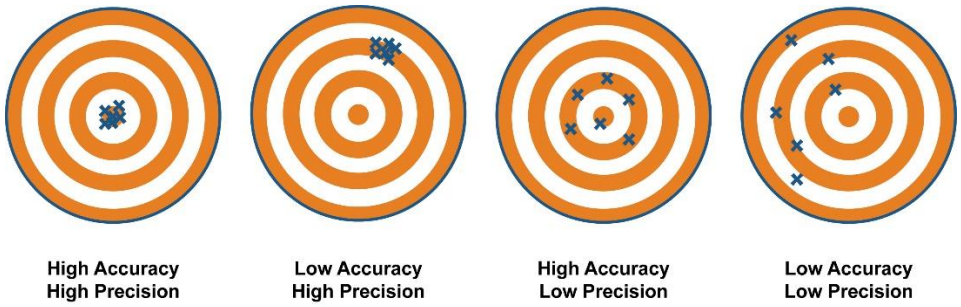

Figure 1: Accuracy and precision description [6]

Precision (or repeatability) of manufacturing processes is crucial to ensure that multiple components can be produced with minimal deviations between them. Accuracy is the closeness of the actual result to the commanded result. See Fig. 1. For WAAM, the accuracy of the printing process geometry is determined by comparing the measured geometry to the CAD model. Precision, on the other hand, compares one print to the next to determine the differences. WAAM has potential to be a mainstream manufacturing process, but it must exhibit sufficient accuracy and repeatability for the production requirements.

Materials and Methods

This study uses a KUKA KR 50 R2500 robot and a Fronius CMT Advanced 4000 welder. ER4943-aluminum wire with a diameter of 1.2 mm is used to deposit the part geometry. The synergic line (i.e., the factory-programmed parameters) used for this deposition is Cold Metal Transfer (CMT) Advanced. The shielding gas is 100% argon with a flow rate of 40 CFH. The welding parameters for this study are provided in Table 1.

Table 1: ER4943-aluminum welding parameters

	Current (A)	Voltage (V)	Wire feed rate (m/min)	Travel speed (mm/s)
First Layer	158.0	15.3	8.0	10.0
Other Layers	149.0	15.1	7.5	10.0

Using the welding parameters specified in Table 1, a bead width of 8 mm and bead height of 3 mm is deposited. The layer height is 2.2 mm and the step over distance is 4.5 mm. These parameters are used for path planning and control the print resolution.

The CAD model in Fig. 2 shows the part geometry printed in this study. There are multiple geometric features that make up the component, including a lower and upper stair as well as a cuboid and cylinder on the upper stair surface. The CAD model is used to establish the nominal values of the print. The geometries of all printed components are compared to one another as well as to the nominal values from the CAD model.

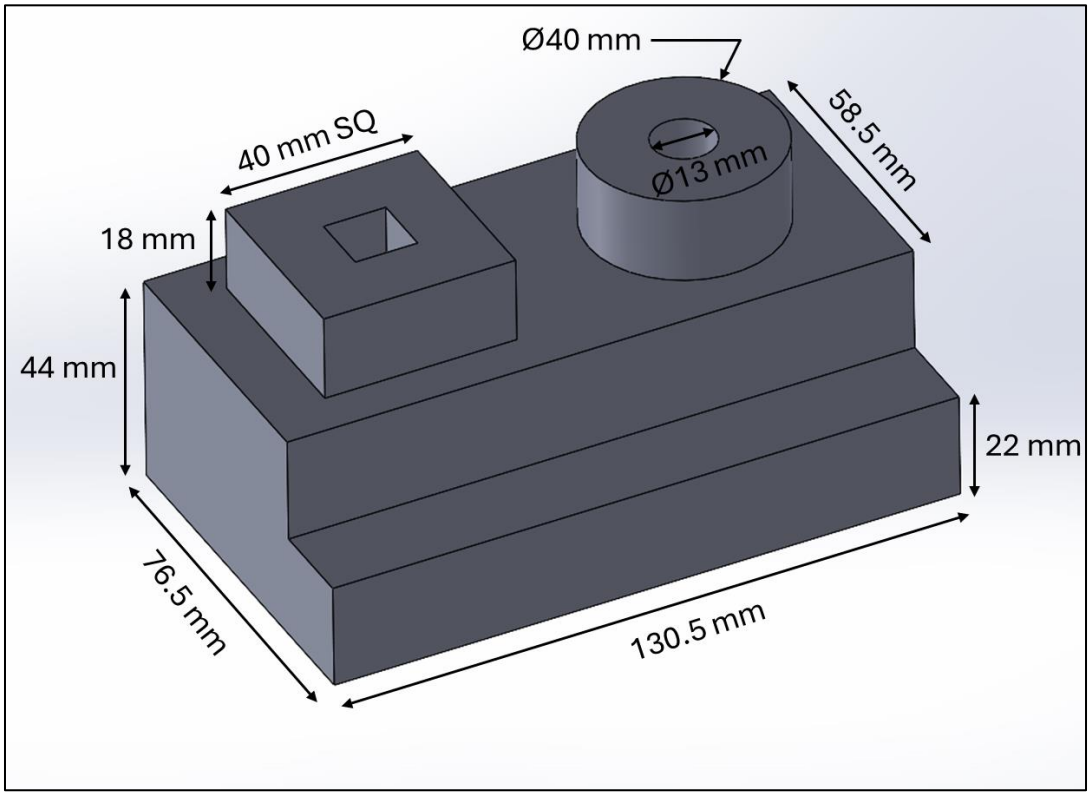

Figure 2: Nominal CAD model

The nominal dimensions for the stair steps are provided in Fig. 2. The lower stair step has a length of 130.5 mm, a width of 76.5 mm and a height of 22 mm. The upper stair step has the same length and height, but has a width of 58.5 mm. This results in an overall height of 44 mm for the two stair steps. The square cuboid has an outer side length of 40 mm, inner side length of 13 mm, and a height of 18 mm. The cylinder has an outer diameter of 40 mm, inner diameter of 13 mm, and a height of 18 mm.

Using Rhinoceros 7 and the Grasshopper plug in, a spiral path was selected for the robot motions [7]. The CAD model was split into multiple STL files to create separate paths for each geometry. Each geometry (lower stair step, upper stair step, cuboid, and cylinder) uses a spiral path where the strike of the arc is initiated at the outer wall and the crater finishes in the middle of the component following the spiral. For the stair steps, the spiral switches direction for each layer where one layer starts on the outer wall and finishes in the middle, and then the next layer starts in the middle and finishes on the outer wall. The spiral path was used because it provides a relatively uniform temperature distribution which helps maintain a level layer height. Also, having one continuous bead for each layer gives minimal strike and crater zones which prevent them from affecting the layer height.

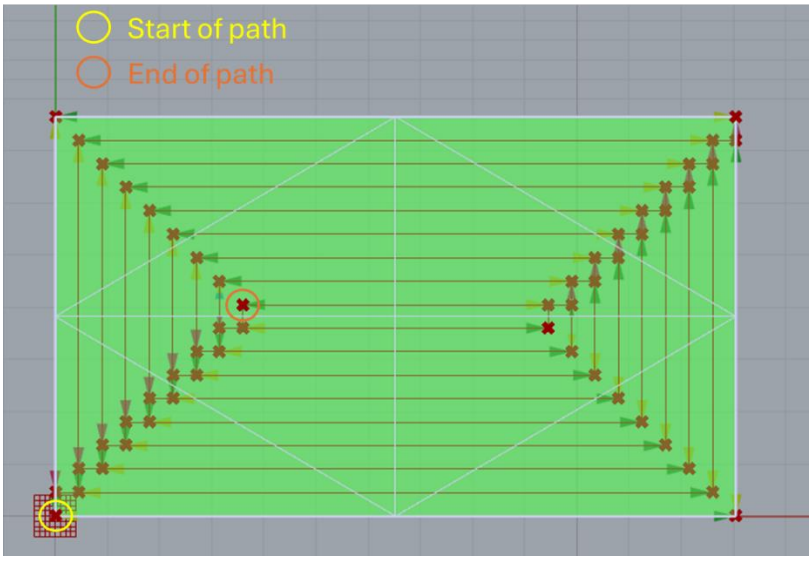

Figure 3: Lower stair step spiral path

Octopuz is a path planning software that enables manipulation of the robot's orientation during deposition [8]. The point cloud developed from Rhinoceros 7 and the Grasshopper plug in is imported into Octopuz and the final path with the correct robot orientations is created. The approximation distance for each point in the path is specified to be 4 mm, which allows the robot to maintain a constant travel velocity of 10 mm/s. The welding job for each layer is specified, where the job contains the welding parameters specified in Table 1.

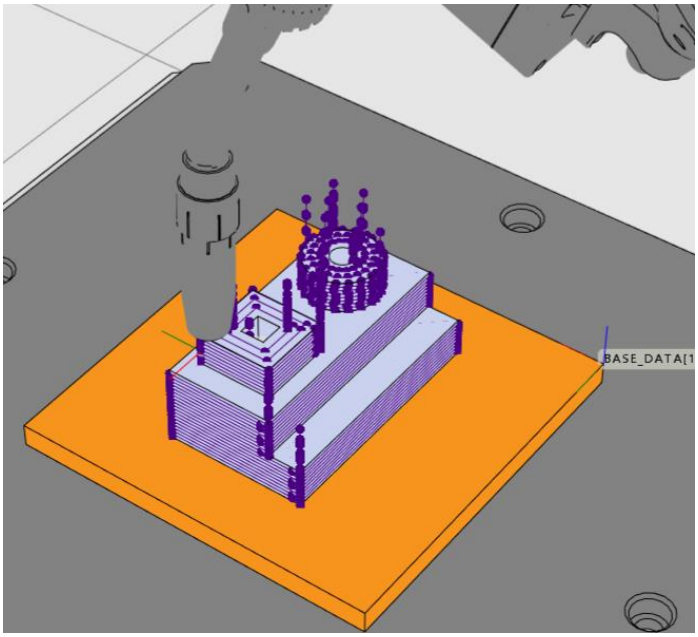

Figure 4: Octopuz path plan

Interpass temperature is monitored throughout the deposition process using a FLIR A65 infrared (IR) camera. The targeted interpass temperature is 85°C for the previously deposited layer's surface temperature. This allows the print to sufficiently cool and maintain a consistent bead geometry and layer height.

The WAAM geometric repeatability is evaluated by printing the same part five times. The same setup, path planning, and interpass temperature is repeated for each print. The geometries of the five nominally identical parts are then evaluated.

After printing five components using the Fig. 2 model to generate the robot paths, the geometric features for each print are measured and compared. The deposited parts are scanned using a ZEISS ATOS Q structured light scanner. An STL model is generated from each scan and compared to the nominal CAD model to determine the accuracy. Each STL model is then compared to the others and deviations between the printed parts are calculated to determine the repeatability.

Results and Discussion

The cycle time for each print is between 5 and 6 hours with a deposition time of 1 hour 24 minutes and a cooling time of about 4 hours. Waiting for the previous deposited surface to reach an interpass temperature of 85°C varied from 2 minutes to 15 minutes, depending on the progress of the build. As the build proceeds, the internal temperature increases, so the time to cool between layers increases.

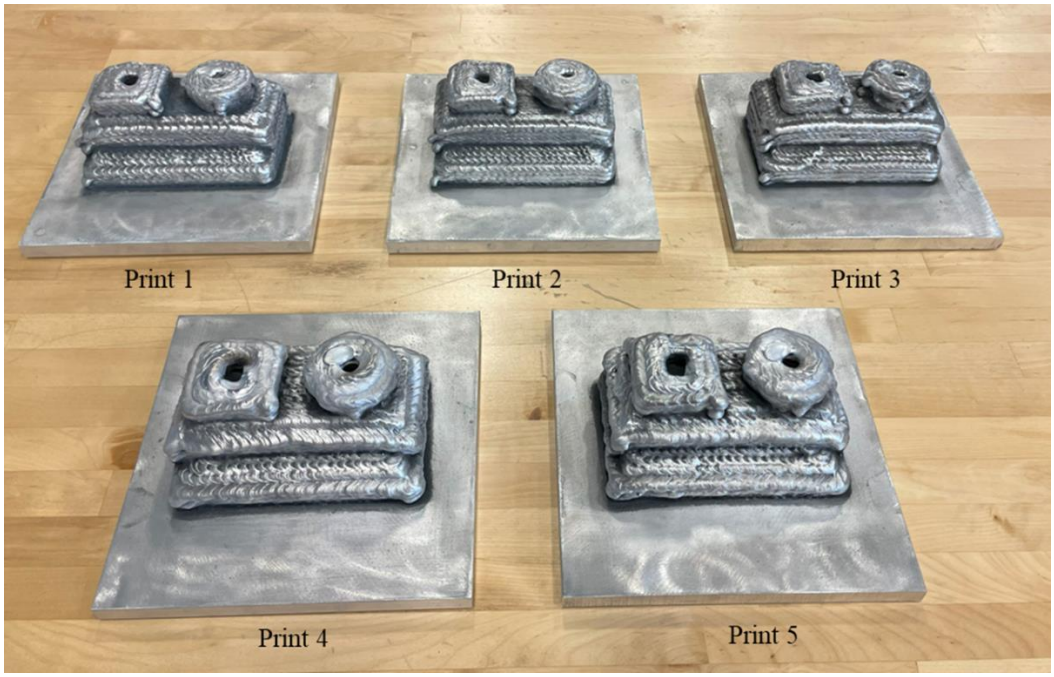

Figure 5: Printed components

After slag removal with a wire brush, the prints are visually similar as shown in Fig. 5. However, the first three prints and the last two prints are slightly different. This is due to a problem with the Robacta drive, specifically the wire feed driver at the welding torch. For prints 1, 2, and 3, the Robacta drive caused the wire to rub which introduced small aluminum shavings into the melt pool. This created more slag on the surface of the prints. The drive was then replaced and resulted in less slag on the surface of prints 4 and 5.

Due to the cleaner welds for prints 4 and 5, the deposited surface appeared cooler than normal throughout the printing process. This was due to the more reflective deposited surface with the decreased slag. The reflectivity changed the emissivity affected the temperature reported by the IR camera. The interpass temperature for prints 4 and 5 was therefore higher and resulted in the sagging at the sides of the prints.

Overall, each print is higher in the middle and lower on the outside edges of the build. All commanded features are observed in each of the five prints.

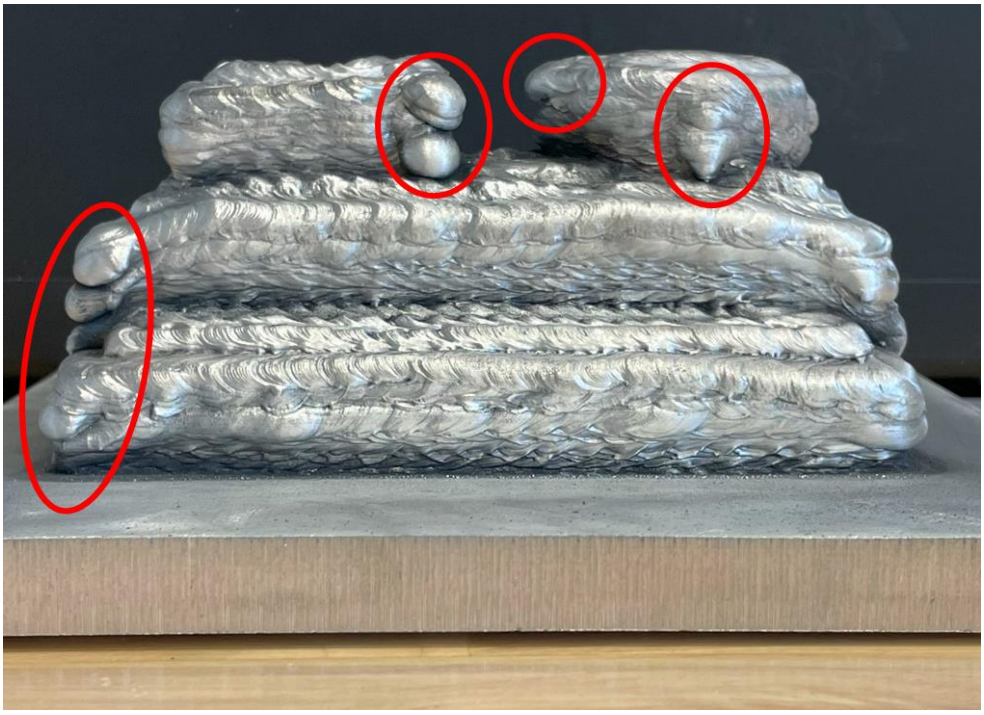

Figure 6: Example strike location surface defects in print 5

Surface defects, such as buildup at the strike location of each layer, can be observed in each print. The strike location results in a local sag because there is more material deposited at the strike to ensure full penetration. Gravity pulls the extra material down causing sagging surface defects at the strike locations. These can be machined away when producing a finished part and, therefore, do not affect the finished part dimensions. However, sufficient material must be present to leave the desired geometry. The strike locations are seen in all the printed parts, which indicates that these defects are repeatable and can be reduced by further testing on the strike and updated path planning.

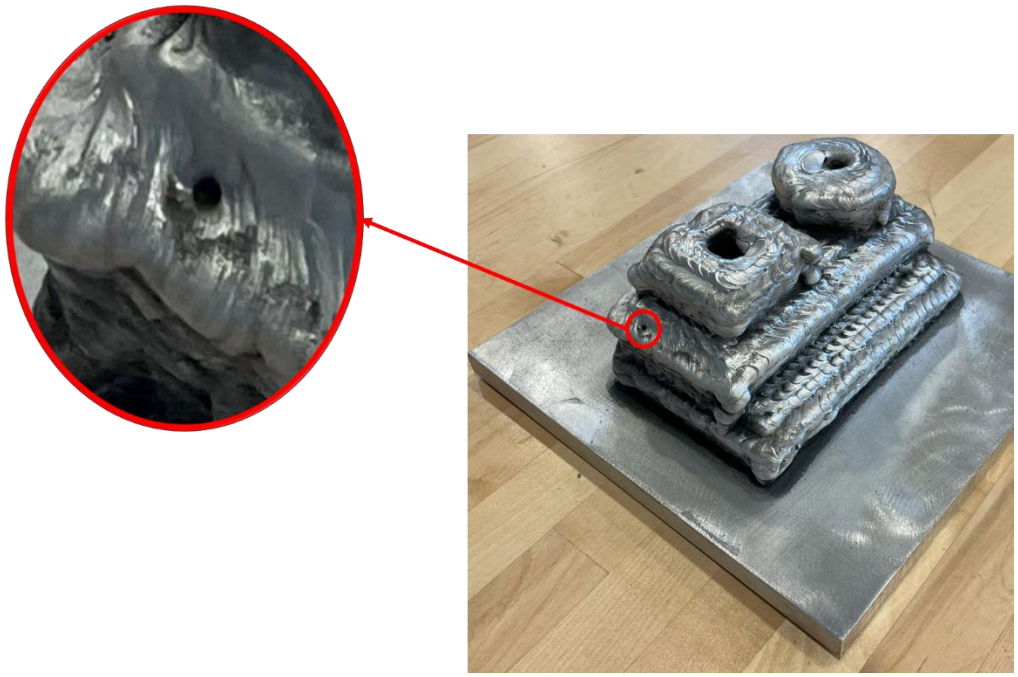

Figure 7: Porosity surface defect in print 5

Porosity on the surface of the printed parts was not typically observed but print 5 did have a small cavity. This was due to the temperature measurement issue causing the print to start at a higher interpass temperature than desired. It led to the sides of the print becoming too underbuilt so that the contact tip to workpiece distance (CTWD) exceeded the typical 18 mm. The increase in CTWD caused incomplete penetration of the weld and created the cavity shown in Fig. 7. The porosity defect was not repeated in other locations, but the underbuilt sagging did repeat.

Each print was scanned using the ZEISS ATOS Q structured light scanner. Scan results are displayed in Fig. 8.

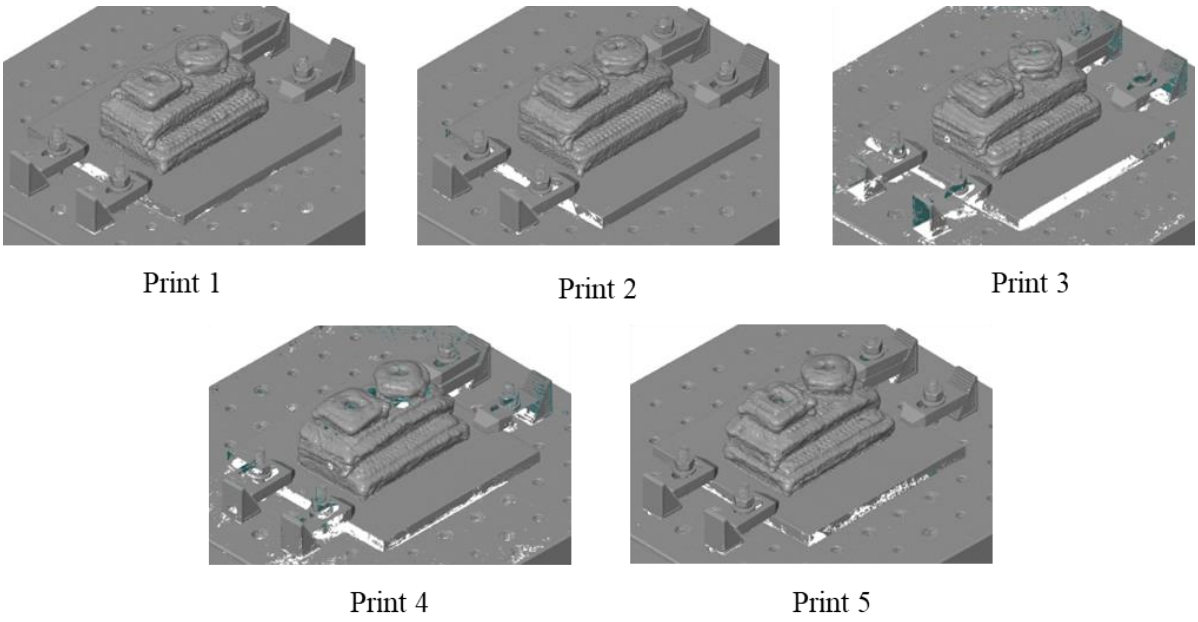

Figure 8: Scanned components

The STL models displayed in Fig. 8 are obtained with the substrate unbolted from the pallet. Each scan is compared to the CAD model using ZEISS Inspect Optical 3D 2023 software [9]. An example for print 1 is shown in Fig. 9 and all the prints are shown in Fig. 10. The deviation labels in both figures show the vector difference from the CAD model to the printed geometry.

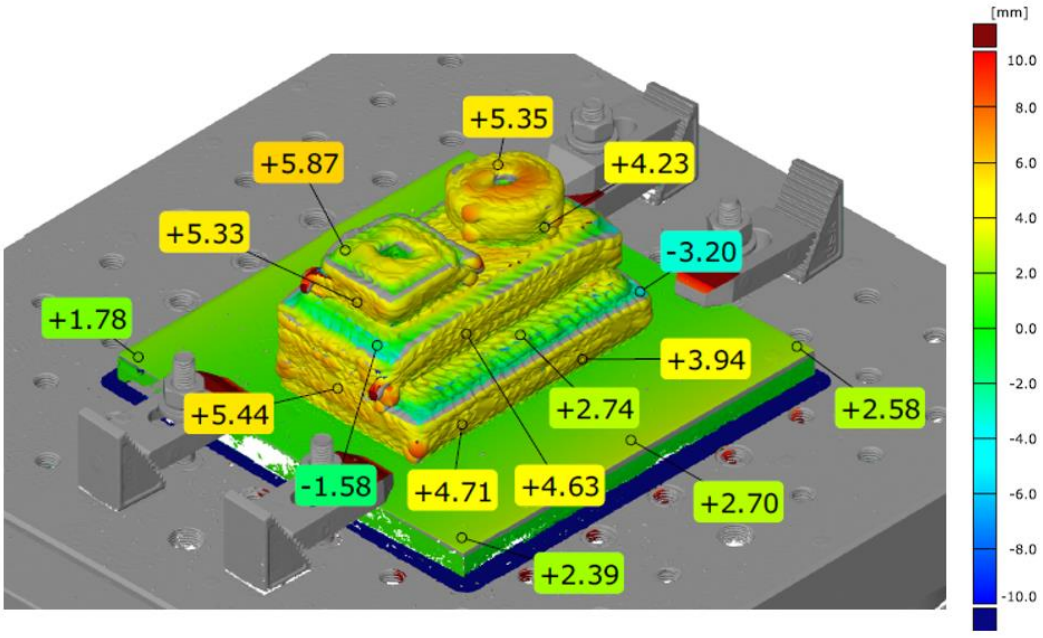

Figure 9: Print 1 surface comparison to CAD model

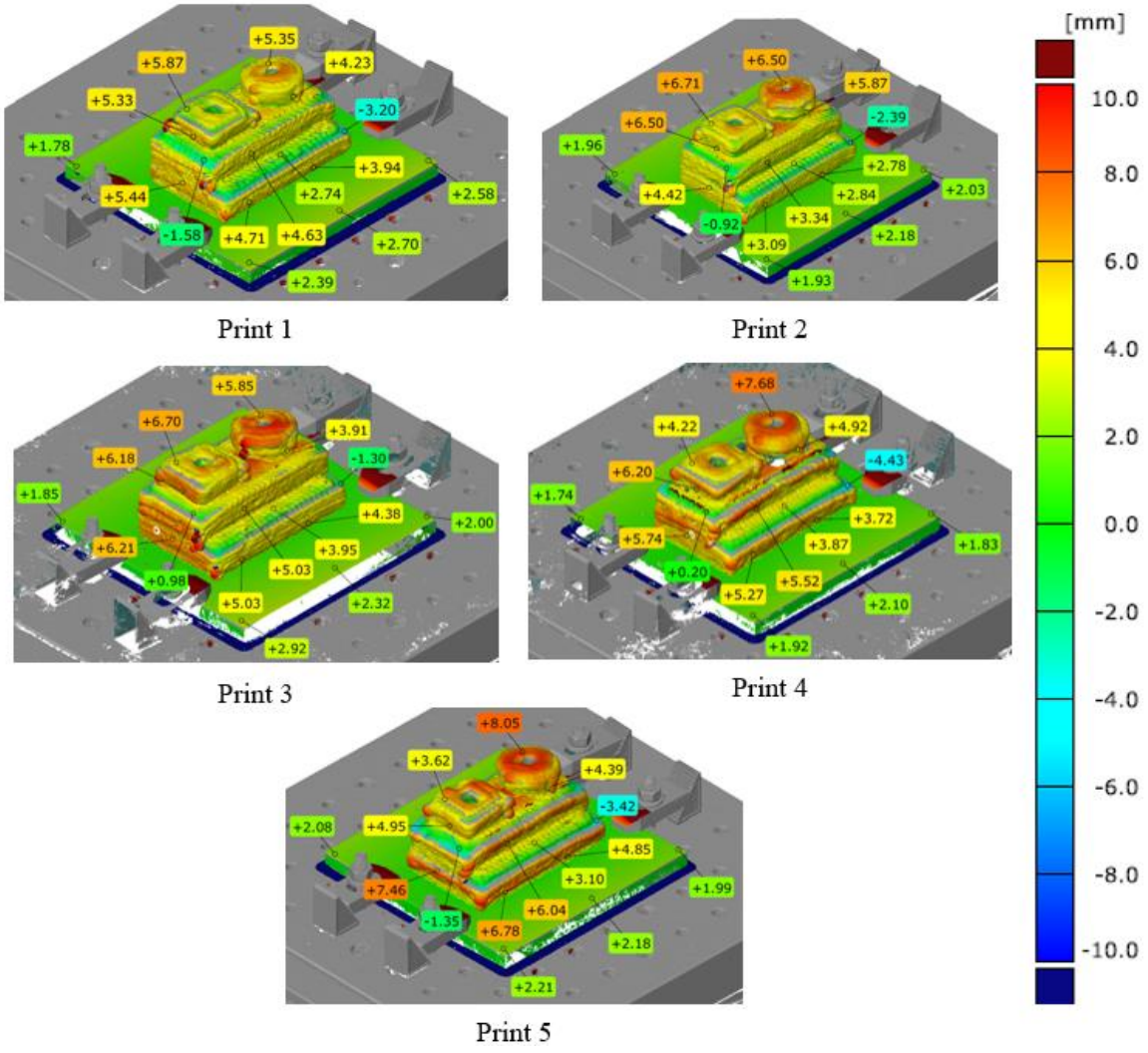

Figure 10: Printed surface comparison to CAD model

In Fig. 10, each scan has deviation labels placed throughout the surface of the build. Using a surface comparison on a scale from -10 mm to 10 mm, each part is compared to the nominal CAD model. Slight differences between each print are seen, but they are all overbuilt or underbuilt at the same locations. This shows that each print is repeatable with only slight deviations from one to the next.

Most of the build volume is overbuilt for each print except at the edges of them. This is where the prints are sagging due to the outer layers depositing at a higher temperature. As the print progresses, the edges slope off. This results in underbuilt edges when compared to the nominal. All the prints illustrate that the process underbuilds at the same locations.

The as-printed dimensions for each geometric feature everyone each print are compared to their nominal values. Using an outer caliper measuring tool in ZEISS Inspect 2023, the outer lengths and widths for every geometric feature are measured. This method excludes the overbuilt strike locations and underbuilt edges. An example of this measurement is seen in Fig. 11, where the measurement for the length of the lower stair from print 1 is shown.

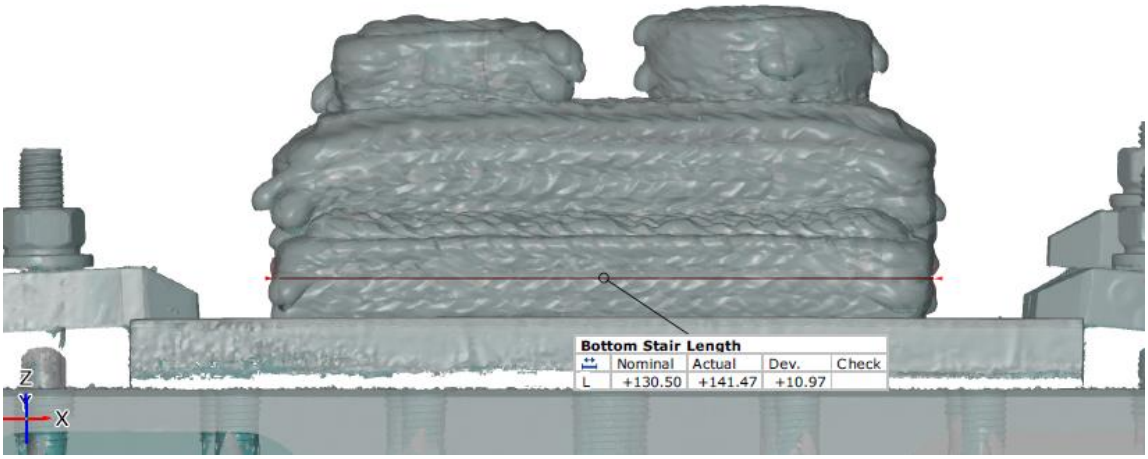

Figure 11: Print 1 lower stair step length measurement

An inner caliper measuring tool is used to measure the inner surface of the cuboid. By fitting a nominal cylinder to the printed cylinder, the inner and outer diameters are measured. Lastly, the height of every geometric feature is measured by fitting a first plane on the top surface of the printed component and a second plane to the measurement surface. Using these methods enables outlier data to be removed and ensures an accurate measurement. The average deviation from nominal for each feature is provided in Fig. 12.

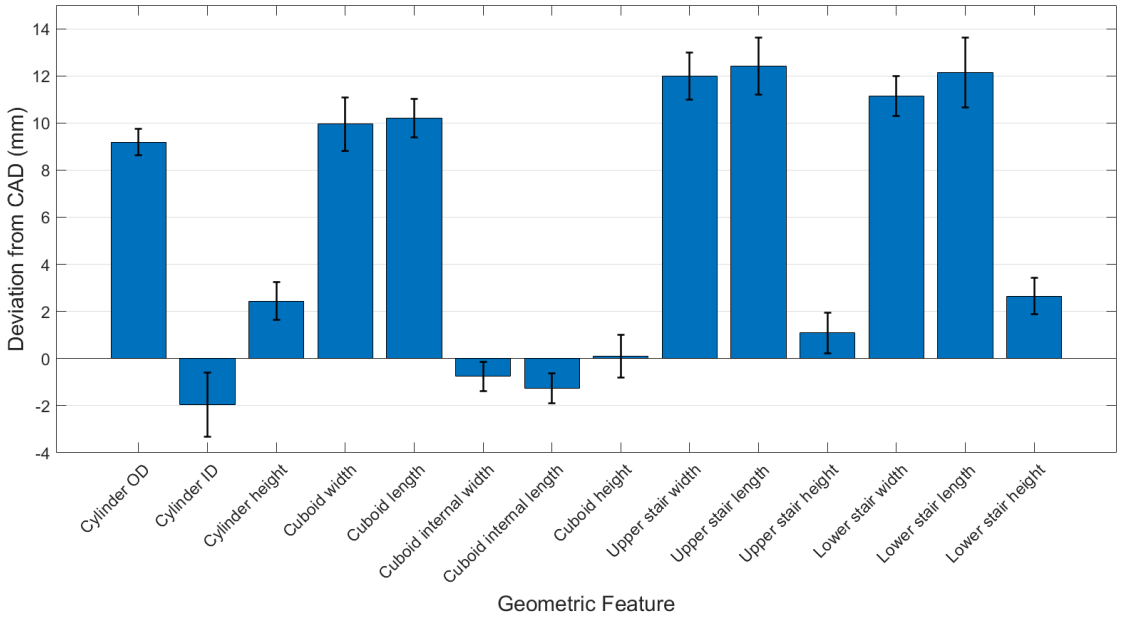

Figure 12: Average deviation of geometric features from CAD

On average, each geometric feature is overbuilt. This is found by measuring each geometric feature for each print and taking the average measured value. The bar graph in Fig. 12 provides the average measured value for each feature and the one standard deviation error bar indicates the deviation between the prints. For internal features, a negative value shows that the hole is smaller than the nominal hole. This means that the printed dimension is overbuilt. For the external features, a positive value defines the printed dimension to be larger than the nominal, again indicating that it is overbuilt. The cylinder outer diameter (OD) and the lengths and widths of all external features are overbuilt by more than 9.19 mm. The cylinder inner diameter (ID) and the internal length and internal width of the cuboid are overbuilt by more than 0.76 mm. The heights for each feature are slightly overbuilt ranging from 0.10 mm to 2.65 mm. The geometries are intentionally overbuilt based on the path planning.

Each geometric feature has its own path. However, the external features are planned to have the middle of the outer bead to be at the nominal value. With a bead width of 8 mm, this causes all external walls to be overbuilt by 4.5 mm on each side. The internal feature's path has an inner bead that is offset to account for the bead width. This is why the internal features are closer to the nominal than the external features. Lastly, the heights for each feature are all slightly overbuilt. The path planned for each height has the last bead at the nominal height. With a bead height of 3 mm and a layer height of 2.2 mm, this accounts for the overbuild being relatively close to the 2.2 mm value. However, the cuboid height is close to the nominal because it has one less layer in its path due to issues with welding to the contact tip.

The error bars in Fig. 12 identify the process repeatability. These show that there are slight deviations in all the geometric features from one print to the next. The smaller the error bar, the

more precise the prints. The cylinder OD has the smallest standard deviation of 0.57 mm resulting in lower and upper limits of 8.62 mm and 9.76 mm relative to the average value of 9.19 mm. The lower stair length has the largest variation between prints. It has a standard deviation of 1.48 mm, resulting in lower and upper limits of 10.66 mm and 13.62 mm relative to the average value of 12.14 mm. The average value of all standard deviations was 0.93 mm, which indicates that the print repeatability is small, and the process is reasonably precise.

The robotic WAAM results demonstrated a low accuracy and high precision (repeatability) printing process. The low accuracy is obtained because the printed part dimensions deviate from the CAD values, but they are overbuilt which means that final machining can produce the desired part geometry and surface finish [10]. The high repeatability is obtained because the geometry of the printed parts is similar from one to the next.

Conclusions

This paper evaluated the process accuracy and repeatability for robotic WAAM of aluminum using CMT. This study was completed by printing the same component five times, scanning each component with a structured light scanner, and comparing the part geometries. It was determined that the average difference from nominal varies from 0.10 mm to 12.40 mm depending on the feature. The standard deviation between prints varied from 0.57 mm to 1.48 mm. The conclusion is that that the process with the parameters described in this paper is repeatable, but not accurate. To improve accuracy, the path planning and welding parameters can be modified. The limiting factor for the repeatability observed in this study was maintaining a consistent interpass temperature.

References

[1] Y. Li, C. Su, and J. Zhu, “Comprehensive review of wire arc additive manufacturing: Hardware system, physical process, monitoring, property characterization, application and future prospects,” *Results in Engineering*, vol. 13, p. 100330, Mar. 2022, doi: 10.1016/J.RINENG.2021.100330.

[2] D. Ding, Z. Pan, S. Van Duin, H. Li, and C. Shen, “Fabricating Superior NiAl Bronze Components through Wire Arc Additive Manufacturing,” *Materials*, vol. 9, no. 8, p. 652, Aug. 2016, doi: 10.3390/ma9080652.

[3] K. E. K. Vimal, M. Naveen Srinivas, and S. Rajak, “Wire arc additive manufacturing of aluminium alloys: A review,” *Mater Today Proc*, vol. 41, pp. 1139–1145, Jan. 2021, doi: 10.1016/J.MATPR.2020.09.153.

[4] J. West, E. Betters, and T. Schmitz, “Limited-constraint WAAM fixture for hybrid manufacturing,” *Manuf Lett*, vol. 37, pp. 66–69, Sep. 2023, doi: 10.1016/J.MFGLET.2023.08.139.

[5] A. Shah, R. Aliyev, H. Zeidler, and S. Krinke, “A Review of the Recent Developments and Challenges in Wire Arc Additive Manufacturing (WAAM) Process,” *Journal of Manufacturing and Materials Processing*, vol. 7, no. 3, p. 97, May 2023, doi: 10.3390/jmmp7030097.

[6] Kent, “Accuracy Vs. Precision.” Accessed: Aug. 04, 2024. [Online]. Available: http://www.kentchemistry.com/links/Measurements/accuracyPrecision.htm

[7] “Rhinoceros 7.” Accessed: Aug. 09, 2024. [Online]. Available: https://www.rhino3d.com/7/

[8] “Octopuz.” Accessed: Aug. 09, 2024. [Online]. Available: https://octopuz.com/

[9] “ZEISS Inspect Optical 3D.” Accessed: Aug. 09, 2024. [Online]. Available: https://www.zeiss.com/metrology/en/software/zeiss-inspect/zeiss-inspect-optical-3d.html

[10] R. Swan, J. Penney, G. Corson, J. Nazario, and T. Schmitz, “Surface location error in robotic milling: Effect of combined low frequency and high frequency vibration modes,” *CIRP J Manuf Sci Technol*, vol. 49, pp. 203–215, Apr. 2024, doi: 10.1016/J.CIRPJ.2024.01.011.